

Imitation learning for sim-to-real transfer of robotic cutting policies based on residual Gaussian process disturbance force model

Jamie Hathaway^{1,2,†}, Rustam Stolkin^{1,2}, Alireza Rastegarpanah^{1,2,†}

Abstract—Robotic cutting, or milling, plays a significant role in applications such as disassembly, decommissioning, and demolition. Planning and control of cutting in real-world scenarios in uncertain environments is a complex task, with the potential to benefit from simulated training environments. This letter focuses on sim-to-real transfer for robotic cutting policies, addressing the need for effective policy transfer from simulation to practical implementation. We extend our previous domain generalisation approach to learning cutting tasks based on a mechanistic model-based simulation framework, by proposing a hybrid approach for sim-to-real transfer based on a milling process force model and residual Gaussian process (GP) force model, learned from either single or multiple real-world cutting force examples. We demonstrate successful sim-to-real transfer of a robotic cutting policy without the need for fine-tuning on the real robot setup. The proposed approach autonomously adapts to materials with differing structural and mechanical properties. Furthermore, we demonstrate the proposed method outperforms fine-tuning or re-training alone.

I. INTRODUCTION

Contact cutting processes feature extensively in a range of applications, most notably manufacturing. However, disassembly applications face particular challenges due to limited availability of Computer-Aided Design (CAD) models, material diversity, and product condition uncertainties. These imply differing challenges from manufacturing as lack of models and prior knowledge about the task introduces challenges for traditional path and process planning approaches. Recently, learning-based approaches have proven successful for online adaptation to uncertainties in a range of application environments, albeit mostly non-destructive [1], [2], [3], [4]. For destructive tasks, simulation environments present a compelling option to avoid the overhead of costly data collection. For example, previous work [5] successfully demonstrated learning and adaptation to a range of uncertain

milling environments; however, challenges remain in sim-to-real adaptation.

While high precision dynamometer setups are extensively used in research applications, challenges are presented for disassembly applications due to geometric limitations and relatively high cost [6], [7]. Force-torque sensors, either mounted at the wrist, or directly integrated into the robot, offer comparatively greater flexibility and lower cost. However, sensor limitations result in considerable differences between simulation and real world from factors such as tool vibration, motor cogging torque and residual unmodelled dynamic effects such as chattering, which are difficult to model without laborious identification. Learning-based approaches suffer poor generalisation when dealing with distributional mismatch between source and target domain observations. Furthermore, direct re-training is problematic due to the problem of catastrophic forgetting, resulting in large reductions in performance [8]. Hence, direct sim-to-real adaptation (i.e. without re-training / direct supervision on the target domain) is desirable due to safety issues and limited sample availability.

This letter proposes an imitation learning based sim-to-real adaptation approach for learning milling tasks based on residual modelling of disturbances directly from offline real world cutting demonstrations. We demonstrate successful sim-to-real transfer of a cutting policy without requirement for supervised domain adaptation on the target domain, based on a series of real world cutting trials on unknown materials. We furthermore demonstrate the proposed framework outperforms fine-tuning or direct re-training alone. The approach is prior-knowledge independent in the sense that only assumption of a periodic disturbance force is made.

The letter is structured as follows: we survey related work in the area of robotic milling, transfer learning and domain adaptation approaches in Section II. Section III introduces the proposed method based on residual Gaussian process modelling of real world cutting examples and knowledge transfer via imitation learning. Section IV details evaluation of the method for simulated and real world cutting trials. Finally, Section V concludes the letter.

II. RELATED WORK

Previous approaches to sim to real adaptation of policies can be broadly categorised into domain adaptive and transfer learning approaches [9]. In the context of reinforcement learning (RL), the aim of the former is to obtain a policy representation that can adapt to the real world via the

¹ Department of Metallurgy & Materials Science, University of Birmingham, Birmingham, UK, B15 2TT.

² The Faraday Institution, Quad One, Harwell Science and Innovation Campus, Didcot, UK, OX11 0RA.

[†] These authors contributed equally to this work.

This work was supported in part by the project called “Research and Development of a Highly Automated and Safe Streamlined Process for Increase Lithium-ion Battery Repurposing and Recycling” (REBELION) under Grant 101104241 and in part by the UK Research and Innovation (UKRI) project “Reuse and Recycling of Lithium-Ion Batteries” (RELIB) under RELiB2 Grant FIRG005 and RELiB3 Grant FIRG057.

The authors would like to acknowledge Abdelaziz Wasfy Shaarawy, Cesar Contreras, Carl Meggs and Christopher Gell respectively for assistance with experimental validation, design of material holder and cutter tool for experiments herein.

This work has been submitted to the IEEE for possible publication. Copyright may be transferred without notice, after which this version may no longer be accessible.

alignment of conditional or marginal distributions of observations between source and target domains. Previously, domain adaptation approaches have been proposed based on unpaired translation models [10]. In [11], a 3-stage framework for imitation learning from visual demonstrations was proposed. Another approach for unsupervised domain adaptation was proposed in [12] based on a deep spherical manifold Gaussian kernel to align source and target domain distributions. Zhao et al. [13] introduces a reinforcement learning-based approach for deformation control in machining across different samples. A joint invariant feature representation is learned for pairs of samples which is used to train a meta-model which adapts to new tasks by fine-tuning. A notable drawback is that for each sample a new policy must be trained to initially generate the meta-model; however, once the meta model is generated, the approach can be fine-tuned with minimal data. A related concept for domain adaptation is proposed in [14] by learning policies within a unified latent space representation of the source and target domain observations.

Another family of approaches focuses on domain adaptation for classification based on a combination of classifier and discriminator models. These are reminiscent of image classification works by leveraging a backbone trained across multiple tasks to generalise across different domains [15]. In [16], this is employed with a weighted combination of global and local discriminators for generalisation of tool wear classification across different milling tools. However, these approaches are still costly in terms of data collection. Consider that in addition to labelled source domain data, a large amount of *unlabelled* target domain data are necessary to train the discriminators. To address the problem of incomplete target domain data, [17] proposed a domain adaptation method for condition monitoring of different milling tools based on a generative CNN. Besides data collection, domain adaptive approaches typically make assumptions about the differences between domains. A common assumption is that the conditional distributions of outputs, such as classifiers, are domain invariant, while differences between the domains arise from differences in the marginal distributions over observations, which is not always the case [18]. In this work, we consider the case that the conditional distributions differ between domains, which represents the “conditional shift” case from [18].

Related to the domain adaptation view on sim-to-real transfer, another approach is to compensate directly for measured disturbances on the real setup. For example, an online disturbance rejection approach is presented in [19] based on a combination of a disturbance observer with a GP regression model of position-based disturbances, while more specifically to milling, [7] proposes a 4-inertial disturbance observer approach for identification of milling force models. However, the authors suggest that some level of prior knowledge may be required to obtain initial estimates for accurate parameter identification.

Transfer learning approaches contrast domain adaptive approaches in that they aim to improve performance on a

target domain via transfer of knowledge between domains. This transfer can be unidirectional (e.g. direct fine-tuning of an existing policy on real world), or bi-directional, such as incorporating knowledge obtained from real world experiments to inform simulation design. Recently, sim-to-real transfer approaches have been proposed based on augmentation of simulations with models learned from trajectories collected from the real environment. In [20] a neural augmented simulation approach was proposed based on a deep neural network dynamic model learned from real world trajectories. Similarly, [21] proposed learning of an inverse dynamics model as a deep neural network for sim-to-real adaptation. However, these approaches require a large number of real world samples to train. On the other hand, Gaussian processes (GPs) have been demonstrated to be efficient at learning from a small number of samples. This has resulted in sim-to-real and domain adaptation approaches in other application areas [22]. Another GP-based approach based on synthesis of data from multiple experts is proposed in [23] for identification of facial expressions, where the target domains are different faces. Alternative sim-to-real transfer approaches have employed system identification methods to optimise physical parameters of a simulation to maximise target domain performance [24]. Therefore, these methods are capable of only modelling parametric differences between source and target domains. Related to this concept and this present work, [25] leverages an imitation-learning-based approach for domain adaptation based on real world demonstrations on a misspecified simulator.

III. METHODOLOGY

A. Dataset Preparation

We consider an initially unstructured dataset comprising time series $\mathcal{D}_u = \{\mathbf{X}_0 \dots, \mathbf{X}_n\}$. Each time series contains force measurements $\mathbf{X}_i = \{\mathbf{f}_e\}$. Many periodic disturbances are parameterised as a function of position instead of time [19]. In the absence of position measurements, the data must first be aligned in the time domain. Each time series is first normalised as:

$$\mathbf{X}_i = \Sigma_{\mathbf{X}_i}^{-1} (\mathbf{X}_i - \bar{\mathbf{X}}_i) \quad (1)$$

where $\bar{\mathbf{X}}_i$, $\Sigma_{\mathbf{X}_i}$ are the mean and standard deviations of each example time series \mathbf{X}_i . The alignment in time domain consists of an initial coarse alignment stage, followed by a fine alignment stage. The coarse alignment is performed by maximising the cross-correlation:

$$t_{\text{delay}} = \underset{t}{\operatorname{argmax}} ((\mathbf{X}_i * \mathbf{X}_j))(t) \quad (2)$$

Subsequently, the fine alignment is performed with pairwise dynamic time warping (DTW) between each example trajectory pair \mathbf{X}_i , \mathbf{X}_j . DTW finds an optimal warping path:

$$(l_n^*, m_n^*) = \underset{(l_n, m_n)}{\operatorname{argmin}} \sum_n \frac{d(\mathbf{x}_{l_n}, \mathbf{x}_{m_n}) w_n}{\sum_{n'} w_{n'}} \quad (3)$$

with respect to a cumulative weighted distance between features $d(\mathbf{x}_l, \mathbf{x}_m)$ (here Euclidean distance), where w_n are

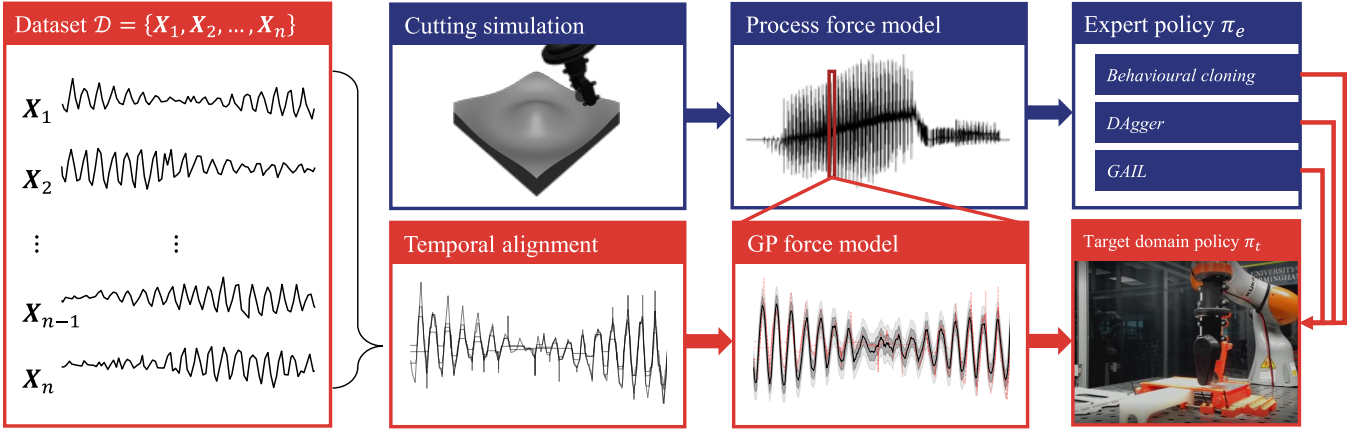


Fig. 1: Overview of the proposed framework.

weighting terms. Adopting the convention from [26], the “symmetric2” step pattern was used. To account for variable length examples, we employ an open-ended DTW approach, which allows for more flexible alignment by permitting variable-length warping paths, which further computes the minimum (3) over all truncated sequences of \mathbf{X}_j . To re-index a time series according to the warping path, each element of the original time series is assigned to a new time point based on the optimal mapping. This re-indexed time series $\hat{\mathbf{X}}$ effectively accounts for time distortions, allowing synchronization and alignment of the data across different examples. Hence, the final dataset comprises aligned time series $\mathcal{D} = \{\hat{\mathbf{X}}_0 \dots, \hat{\mathbf{X}}_n\}$.

B. GP Force Model

We consider the regression problem:

$$\mathbf{f}_e = \mathbf{f}(t) + \mathbf{d}(t) + \epsilon \quad (4)$$

where $f(t)$ represents the force computed from the underlying process force model, while $d(t)$ represents a disturbance force. The disturbance $d(t)$ is assumed to be periodic and with independent and identically distributed (i.i.d) noise $\epsilon \sim \mathcal{N}(0, \sigma^2)$. We model the disturbance force $d(t)$ as a Gaussian Process (GP) with zero mean and covariance function $k(\mathbf{x}, \mathbf{x}')$

$$\mathbf{d}(t) \sim \mathcal{GP}(\mathbf{0}, k(\mathbf{t}, \mathbf{t}')) \quad (5)$$

where the distribution of observed and unobserved data is modeled as a joint multivariate Gaussian distribution:

$$\begin{bmatrix} \mathbf{d} \\ \mathbf{d}_* \end{bmatrix} = \mathcal{N}\left(\mathbf{0}, \begin{bmatrix} \mathbf{K} & \mathbf{K}_* \\ \mathbf{K}_*^\top & \mathbf{K}_{**} \end{bmatrix}\right) \quad (6)$$

where \mathbf{K} , \mathbf{K}_* , \mathbf{K}_{**} are the training, train-test and test covariance matrices respectively. The posterior predictive distribution for the disturbance force \mathbf{d}_* given test points \mathbf{X}_* is then

$$p(\mathbf{d}_* | \mathcal{D}, \mathbf{d}, \mathbf{X}_*) = \mathcal{N}(\boldsymbol{\mu}, \boldsymbol{\Sigma}) \quad (7)$$

$$\boldsymbol{\mu} = \mathbf{K}_*^\top [\mathbf{K} + \sigma^2 \mathbf{I}]^{-1} \mathbf{d} \quad (8)$$

$$\boldsymbol{\Sigma} = \mathbf{K}_{**} - \mathbf{K}_*^\top [\mathbf{K} + \sigma^2 \mathbf{I}]^{-1} \mathbf{K}_* \quad (9)$$

To capture the periodic nature of the disturbance force, we use the exponential sine covariance function

$$k(\mathbf{x}, \mathbf{x}') = \exp\left(-\frac{2 \sin^2\left(\frac{\pi d(\mathbf{t}, \mathbf{t}')}{p}\right)}{l^2}\right) \quad (10)$$

with periodicity p , length scale l and Euclidean distance $d(\mathbf{t}, \mathbf{t}')$.

Based on the assumptions of the mechanistic force modelling approach [27], the cutting force \mathbf{f} can be related to each cutting edge $p \in 1 \dots N_p$ of a fluted cutting tool via mechanistic constants \mathbf{k}_c , \mathbf{k}_e :

$$\mathbf{f}^p = b_p \mathbf{k}_e + b_p \mathbf{k}_c h_p \quad (11)$$

where b_p is the thickness of the cutting edge, h_p is the uncut chip thickness, computed from the cutting edge rotation angle θ_p in the tool model reference frame, tool feed rate v and spindle speed ω :

$$h_p = \sin \theta_p \frac{v}{N_p \omega} \quad (12)$$

The total cutting force is computed as the sum over cutting elements weighted by the Boolean vector $\mathbf{G} \in \mathbb{B}^{N_p}$ specifying the engagement of each element k with the workpiece.

$$\mathbf{f} = \sum_p^{N_p} G_p \mathbf{R}_p \mathbf{f}^p \quad (13)$$

where \mathbf{R}_p is the rotation of cutting edge p about the tool axis to the tool model frame.

C. Imitation Learning Framework

The cutting task is formulated in the Mujoco simulation environment, into which the model of cutting mechanics from (13) is embedded. The expert reward function r expresses a weighted sum of task-specific performance metrics MRV (material removed volume) and cutting time t_{cut} , and feasibility reward shaping comprising path error e , process force \mathbf{f}

$$r = Q_{\text{MRV}} \cdot \text{MRV} - Q_{\text{cut}} t_{\text{cut}} - e \mathbf{Q}_d \mathbf{e}^\top - \mathbf{f} \mathbf{Q}_f \mathbf{f}^\top \quad (14)$$

with observations $\mathbf{o} = [\dot{\mathbf{c}}(t) \dot{\mathbf{v}}_{EE}^T \ \mathbf{e} \ \mathbf{v}_{EE} \ \mathbf{f}_e \ \mathbf{a}]^T$, where $\mathbf{c}(t)$ is the reference cutting path, end-effector velocity \mathbf{v}_{EE} , and agent actions \mathbf{a} . Due to the problems of catastrophic forgetting with fine-tuning and high cost of data collection in the real environment, we propose an imitation-learning based approach to train a target policy that can adapt to the target domain via a surrogate target domain. We establish a test case comprising “offline” and “online” imitation learning algorithms; behavioural cloning (BC) and DAgger, which we contrast with the case of the expert policy directly transferred with no fine-tuning, and the expert with fine-tuning directly on the surrogate target domain.

During training, we employ the source domain expert policy π_e to train a surrogate target domain policy $\hat{\pi}_t$. To resemble the fine-tuning case, we initialise the target domain policy as $\hat{\pi}_t = \pi_e$. At each step, the tuple $(\mathbf{o}_e, \pi_e(\mathbf{o}_e))$ is sampled from the base environment using the data collection policy

$$\pi_d = \beta \pi_e + (1 - \beta) \pi_t \quad (15)$$

where β is the non-expert action probability, which is non-zero for DAgger and zero otherwise. Then, the expert observations \mathbf{o}_e , actions \mathbf{a} (\mathbf{o}_e, \mathbf{a}) are modified by sampling from the posterior distribution (7) for each point in the trajectory to generate new experiences $(\mathbf{o}_t, \mathbf{a})$. Subsequently, the surrogate target domain experiences are used to update the target policy as the standard behavioural cloning procedure. However, the method is applicable to other imitation learning algorithms such as GAIL or AIRL. This procedure is summarised in Algorithm 1. We employ the proximal policy optimisation (PPO) algorithm for learning and fine-tuning of policies, although the principles are independent of learning algorithm. For each approach, we conduct training with all strategies for 50 episodes, a learning rate of 1×10^{-3} and batch size of 64. For DAgger, β is varied according to a 0–1 linear schedule for 45 episodes.

Algorithm 1 Imitation-learning sim-to-real transfer

```

Expert policy,  $\pi_e$ , target policy  $\hat{\pi}_t$ 
Source domain (expert) environment  $\mathcal{E}$ 
Disturbance model  $p(\mathbf{d}'|\mathcal{D}, \mathbf{x}, \mathbf{d}, \mathbf{x}')$ 
 $\hat{\pi}_t \leftarrow \pi_e$ 
for  $i = 0$  to  $N$  do
  while episode not done do
    Sample  $(\mathbf{o}_e, \pi_e(\mathbf{o}_e))$  from  $\mathcal{E}$ 
    Sample  $\mathbf{d}' \sim p(\mathbf{d}'|\mathcal{D}, \mathbf{x}, \mathbf{d}, \mathbf{x}')$ 
     $\mathbf{o}_t \leftarrow \mathbf{o}_e + \mathbf{d}'$ 
    Append  $\mathcal{D}_e$  with  $(\mathbf{o}_t, \pi_e(\mathbf{o}_e))$ 
    Update  $\mathcal{E}$  with  $\mathbf{a} \sim \hat{\pi}_t(\mathbf{o}_e)$ 
  end while
end for
Train  $\hat{\pi}_t$  with  $\mathcal{D}_e$  as BC, DAgger, ...

```

D. Experimental Setup

The real world setup consists of a KUKA LBR *iiwa* R820 14kg collaborative robot equipped with a wrist mounted

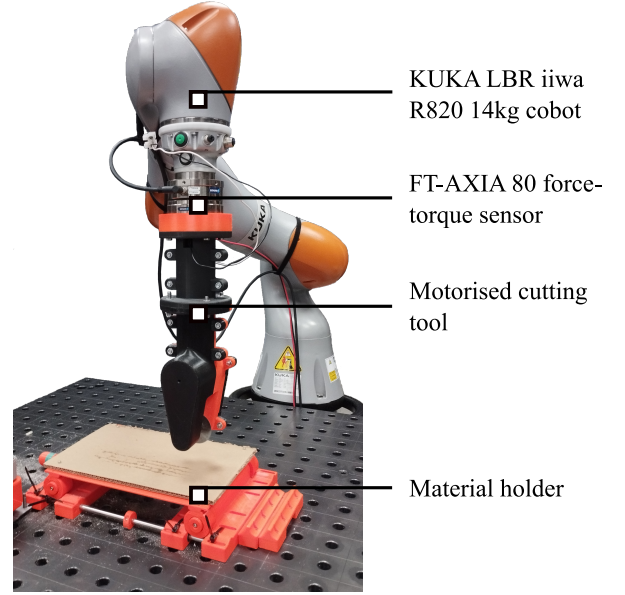


Fig. 2: Overview of the experimental setup used for real world cutting experiments.

motorised slitting saw tool. Although the *iiwa* has built-in torque sensing capabilities, we consider the case where a force-torque sensor (FT-AXIA 80) is mounted between the cutter tool and the robot flange which measures the process force. The policy controls the robot via an operational space computed torque tracking controller, with control law:

$$\boldsymbol{\tau} = \mathbf{J}^T [\boldsymbol{\Lambda}(\mathbf{q}) [\mathbf{K}_d(t) \dot{\mathbf{e}} + \mathbf{K}_p(t) \mathbf{e}] + \boldsymbol{\Gamma} + \boldsymbol{\mu}] \quad (16)$$

where $\boldsymbol{\tau}$ are the commanded joint torques, \mathbf{J} the robot Jacobian, and $\boldsymbol{\Lambda}$, $\boldsymbol{\Gamma}$, $\boldsymbol{\mu}$ the robot dynamic parameters corresponding to inertia, Coriolis / centrifugal forces and gravitational forces respectively. The policy outputs correspond to the controller translational stiffness \mathbf{K}_p and translational setpoint adjustment, consisting of a feed rate modification from a nominal feed rate and depth of cut (DoC) offset from the reference trajectory. The damping gain \mathbf{K}_d is computed according to give a critically damped behaviour for the selected stiffness. For each strategy, we consider a single cutting pass of a planar material by conventional milling. The reference tool path is defined with respect to the material surface position, with a reference DoC of 0mm – hence, the actual DoC is directly selected via the policy DoC offset.

IV. RESULTS & DISCUSSION

In this section, the performance of the proposed method is evaluated in simulation in the context of the performance of the expert in the source domain (i.e. simulation without GP augmentation) and surrogate target domain (simulation augmented with GP). The performance and behaviour is subsequently compared for the true target domain for a series of real world cutting tasks.

A. Simulation studies

We first establish a case study for cutting of a planar material from a set of 50 trials with randomly chosen mechanistic

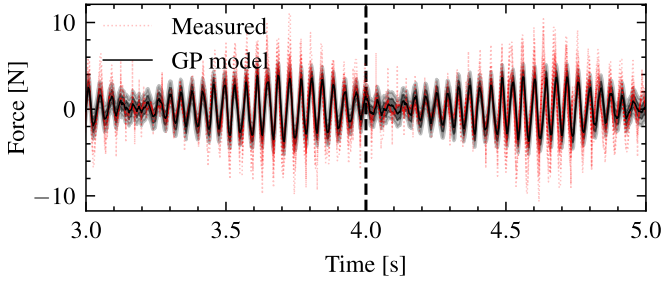


Fig. 3: Plot of measured disturbance force in feed (Y) direction from dataset of examples after temporal alignment. The Gaussian process model fit is shown; the shaded areas show 1- σ and 2- σ standard deviations from the mean respectively. The dashed line shows the transition from training data (left) to extrapolation (right).

constants for the simulation augmented with the learned GP model. We compare the performance of the “expert” agent, which is trained in the unaugmented simulation for 32000 episodes and examine the behaviour with respect to the policies trained with the proposed GP + imitation strategy, with the performance in the base case, i.e. unaugmented simulation as a benchmark. Figure 4 shows the actions adopted by each strategy, consisting of the relative feed rate versus the nominal (0.75m/min), DoC and controller stiffness K_p . Correspondingly, the path deviations in the transverse (e_x) and normal (e_z) directions are shown, along with forces in the feed and normal directions (F_y , F_z respectively).

From Figure 4a the behaviour of the expert in the source domain can be seen. When transferred directly into the surrogate target domain (“Expert GP”), the policy reacts aggressively to the added disturbance, exhibiting sporadic variations in feed rate and stiffness selection. In comparison, the surrogate target domain policies trained with both imitation learning strategies closely tracks the source domain expert behaviour. Conversely, while the actions adopted by the original expert policy after fine-tuning differ, particularly for the stiffness Z component, however, the fine-tuned policy remains similarly sensitive to the disturbances. Comparing the states in Figure 4b further corroborates the similar performance achieved by both imitation learned policies, with DAgger tracking the expert behaviour more closely than BC. The fine-tuned policy adopts a pattern to the expert as directly applied to the surrogate target domain, with a delay of ~ 0.1 s. As an aside, note that with low-pass filtering of the forces, the underlying trend, as seen in the “expert” evaluation, is not recovered, even with aggressive cutoff. This also has the effect of introducing delay into the measured signal; for example, a 10th-order Butterworth filter with a cutoff defined at 5Hz has a maximal group delay of ~ 0.5 s, or 25 policy evaluations.

Broadly, for all strategies, similar patterns in actions can be observed during each phase of the cutting task. For example, the policy adopts a high stiffness and feed rate broadly around the nominal during approach, followed by transitioning to a high feed rate and low stiffness in the normal direction (Z) after impact. Furthermore, the DoC remains consistent across all trials. Therefore, the comparison of each

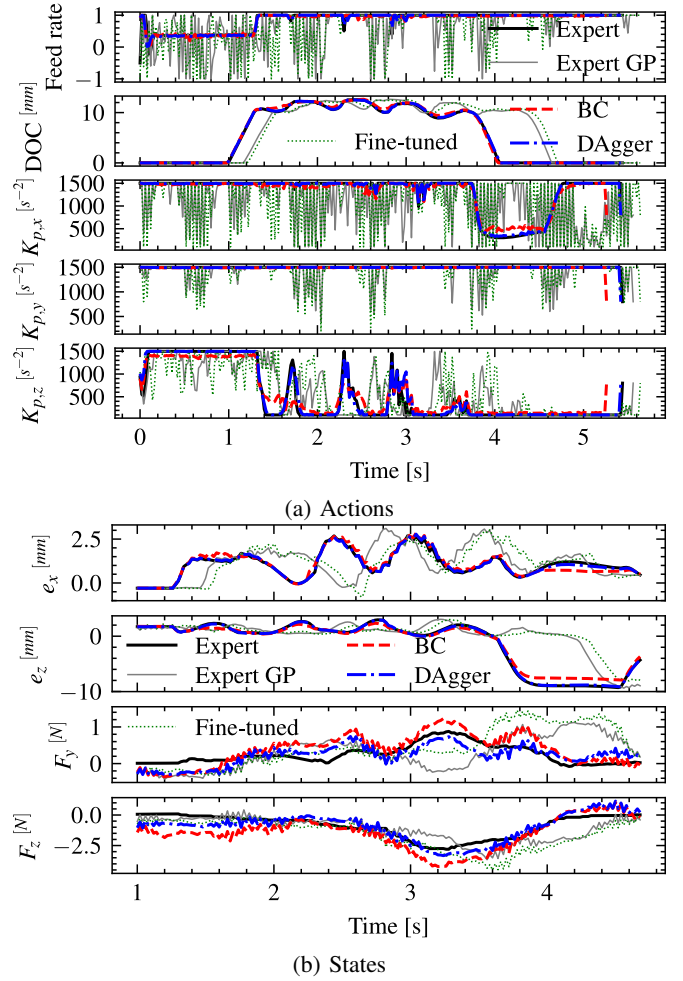


Fig. 4: Comparison of policy actions and states between source domain expert in source and surrogate target domains (Expert, Expert GP), and surrogate target domain policies using fine-tuning, behavioural cloning (BC) and DAgger imitation learning strategies. States include the path error transverse e_x and normal e_z to the planned path and forces in the feed F_y and normal direction F_z . Forces are shown with a 50-point (1s) moving average filter.

strategy implies predominantly *behavioural* benefits of the proposed approach, rather than fundamentally altering the “decision-making” of the original expert strategy.

Figure 5 shows the training curves for expert policies trained from scratch in source and surrogate target domains respectively. The source policy converges rapidly in the first 3M training steps, before a phase of gradual improvement over the remaining 13M steps to a final reward of -0.766. For the surrogate target policy, an initial reduction in performance is recorded, followed by gradual improvement from steps 5.5–12M until convergence to a final reward of -2.24. Besides the advantage of training time reduction (50 episodes vs. 32000, $\sim 0.16\%$ of training time), the final rewards from the surrogate target expert policy are notably reduced. This follows from the inclusion of the GP model representing a more challenging task for the agent; the force observations in particular are directly related to the reward and encode important information about the interaction which relates to

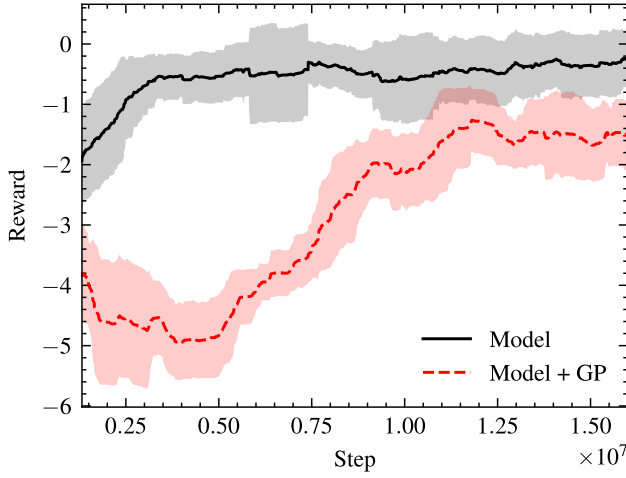


Fig. 5: Comparison of training curves between base environment and environment with GP residual force model.

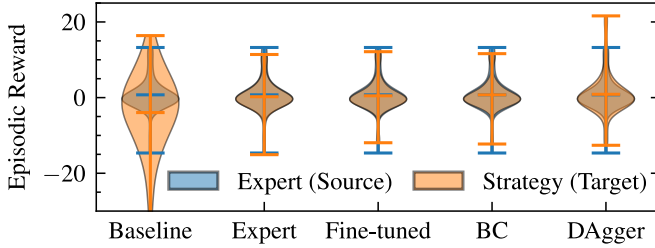


Fig. 6: Violin plot of reward distribution between source domain expert policy and target domain strategies – fixed process parameters for all materials (baseline), unmodified and fine-tuned expert policies, and target policies trained with BC and DAgger imitation learning approaches.

the selection of milling process parameters.

We consider the performance of the original expert policy, the target domain fine tuned policy and policies with each imitation learning strategy (BC, DAgger) in both the original simulation environment and simulation augmented with the learned GP model from real-world trials. We additionally compare the performance with fixed process parameters (Baseline) at the nominal (feed rate 0.75m/min and 1mm DoC) for all materials. In each instance, we compare the episodic rewards over 50 simulation rollouts. From Figure 6 it is clear that the overall performance of the expert and all strategies is robust to distributional mismatch between source and target domains. For the fine-tuned, BC and DAgger strategies, the performance is slightly more consistent in the extreme case as indicated by the higher minimum rewards obtained. The greatest deviation is observed for the DAgger trained target policy from the expert for both the original and GP-augmented environments. As DAgger allows for the trajectories to deviate from those obtained using the expert demonstrations alone, it enables the policy to explore and adapt further to the surrogate target domain. It is therefore unsurprising that DAgger demonstrates superior performance in this case.

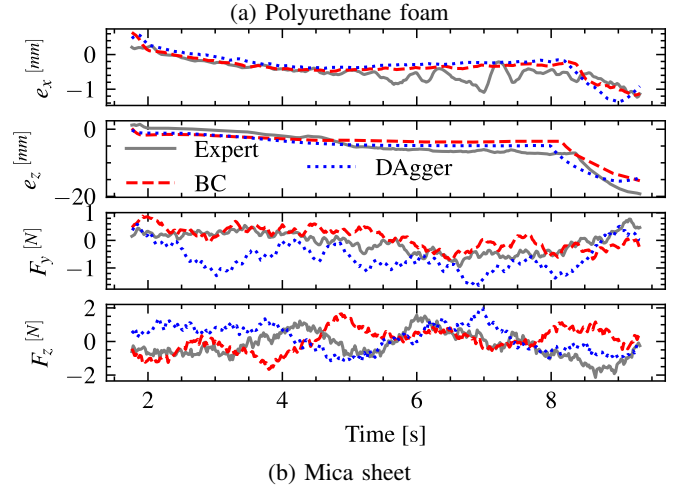
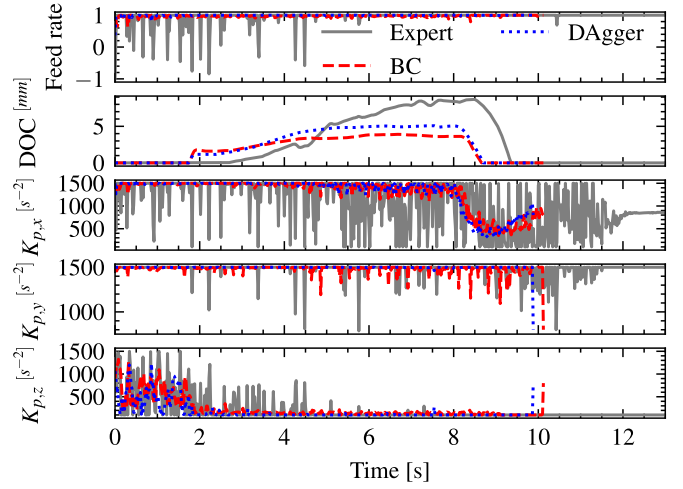


Fig. 7: Comparison of policy actions between source domain expert and surrogate target domain policies using behavioural cloning (BC) and DAgger imitation learning strategies. Actions include the relative feed rate adjustment vs. nominal (0.75m/min), depth of cut (DoC) and controller stiffness K_p .

B. Real world cutting trials

We evaluate the cutting policy for conventional milling of 5 different materials – mica, cardboard, corrugated plastic, high-density polyurethane (PU) foam and aluminium – which exhibit broadly differing mechanical and structural properties. Figure 7 and Figure 8 show the actions and key states for the expert, BC and DAgger trained policies for foam and mica. Emblematic of the source domain expert as applied directly to the real world is a high degree of variability in the agent actions over time, particularly of the controller stiffness K_p , corroborating the behaviour observed in simulation. Selection of feed rate appears sporadic and largely uncorrelated to any particular evolution of the cutting process; for example, an increase in loading of the tool. This can be contrasted with the feed rate selection of the DAgger trained policy, where reductions in feed rate are associated with increases in the DoC due to increased loading on the tool. The behaviour of the expert policy is inconsistent, with path error and force progressively increasing during

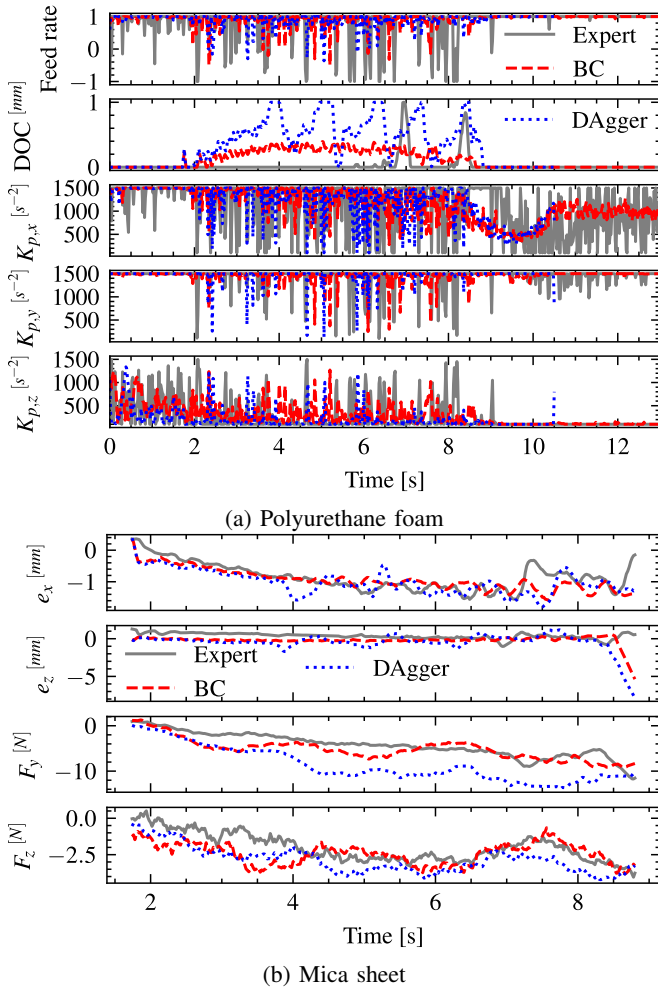


Fig. 8: Comparison of path error transverse e_x and normal e_z to the planned path and forces in the feed F_y and normal direction F_z between source domain expert, BC and DAgger surrogate target domain policies. Forces are shown with a 50-point (1s) moving average filter.

the cutting task, whereas for the BC and DAgger policies, these are relatively consistent. However, it is important to note that since the focus of this work is on “rough” cutting for disassembly or decommissioning applications, and not on achieving high dimensional tolerances, the expected errors are higher than would be expected for milling, e.g. for a manufacturing application.

Some behavioural characteristics are not preserved from the simulation case study; for example, the selected feed rate during the approach stage of cutting remains nearly at the maximum for all strategies, contrasting the with simulation case. Similarly, the stiffness along the normal direction (Z) is increased during the approach phase, however to a lesser extent than in simulation. However, during the cutting phase, these are broadly more similar to the simulation case. As previously established, the force observations encode key information about the interaction, including the discrimination of contact and non-contact states.

A comparison of the average rewards over all materials

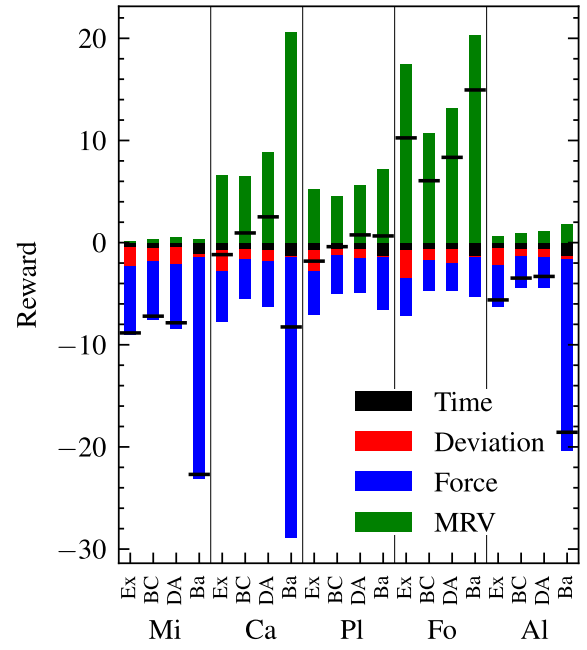


Fig. 9: Breakdown of average reward and reward components by material and strategy. The performance of each strategy, labelled “Ex”, “BC”, “DA” and “Ba” respectively are grouped by the material; here abbreviated Mica, Cardboard, Plastic, Foam and Aluminium respectively. The total reward components for each strategy (i.e. total reward) is marked.

for the expert policy and BC and DAgger trained target policies is shown in Figure 9. Across all trials, consistently lower forces are encountered with the policy-based approach, with higher total rewards observed for all materials with the exception of foam. Similarly, this trend is observed between the expert and imitation-trained policies, while (excluding foam) retaining similar or improved MRV across the range of materials, implying an improved capability to regulate the cutting force for the real world case studies. For overall rewards, a significant difference in between the BC and expert was found for mica (unpaired two-tailed T-test, $p = 0.015$; 95% significance level), with the observed effect being improvement, but not for DAgger ($p = 0.33$); the higher MRV and force implying a more aggressive behaviour. In cardboard, significant differences were found in both cases (BC $p = 0.021$, DAgger $p = 0.020$), with the observed effect being improvement in both cases. For plastic, mixed results are seen (BC $p = 0.14$, DAgger $p = 0.038$) consisting of inconclusive improvement for BC, but observed improvement in the DAgger case. Similarly for foam, BC performed worse than DAgger, differing markedly from the expert with a reduction in reward, ($p = 0.00014$), with an inconclusive difference in performance for DAgger ($p = 0.084$). Finally for aluminium, both strategies showed a self-consistent improvement over the expert, but individually were inconclusive ($p = 0.094$, $p = 0.090$). Overall, it can generally be said that DAgger performed better on the softer materials, whereas BC performed well on stronger materials

such as mica. For DAgger, the performance on the range of case studies was either improved, or – in the least case – did not significantly differ from the expert. This can similarly be said for BC with the exception of foam.

V. CONCLUSION

An imitation-learning based approach for sim-to-real transfer of a robotic cutting policy was proposed. We demonstrate how the residual process dynamics and disturbances can be modelled from a small number of real world trials. We validate the proposed method on a real robot setup, demonstrating the policies transferred to the real world in many cases to have significantly improved performance over the expert as directly transferred from simulation. Furthermore, the behavioural characteristics of the target domain policies (sensitivity to disturbances) were improved. We also demonstrate the proposed method based on imitation learning outperforms fine-tuning or re-training alone, and that improvements can be obtained even with relatively simple offline imitation learning approaches.

A notable limitation of this work is that while the proposed method can incorporate data from multiple examples, the disturbances are assumed to be sampled from the same underlying process. If the disturbances differ between demonstrations, the alignment between demonstrations will be poor. In this case, a separate GP model would be required for each variation. The assumption of a periodic disturbance force furthermore remains a notable limitation. To address these limitations, future work will explore direct synthesis of surrogate real-world data from a minimal unstructured dataset of offline demonstrations.

REFERENCES

- [1] C. C. Beltran-Hernandez, D. Petit, I. G. Ramirez-Alpizar, and K. Harada, "Variable compliance control for robotic peg-in-hole assembly: A deep-reinforcement-learning approach," *Applied Sciences*, vol. 10, no. 19, 2020.
- [2] Y. Wang, C. C. Beltran-Hernandez, W. Wan, and K. Harada, "Hybrid trajectory and force learning of complex assembly tasks: A combined learning framework," *IEEE Access*, vol. 9, pp. 60 175–60 186, 2021.
- [3] X. Li, J. Xiao, W. Zhao, H. Liu, and G. Wang, "Multiple peg-in-hole compliant assembly based on a learning-accelerated deep deterministic policy gradient strategy," *Industrial Robot: the international journal of robotics research and application*, vol. 49, no. 1, pp. 54–64, Jan 2022.
- [4] X. B. Peng, M. Andrychowicz, W. Zaremba, and P. Abbeel, "Sim-to-real transfer of robotic control with dynamics randomization," in *2018 IEEE International Conference on Robotics and Automation (ICRA)*, 2018, pp. 3803–3810.
- [5] J. Hathaway, A. Rastegarpanah, and R. Stolkin, "Learning robotic milling strategies based on passive variable operational space interaction control," *IEEE Transactions on Automation Science and Engineering*, pp. 1–14, 2023.
- [6] B. Gibson, C. Cox, M. Aguilar, A. Strauss, and G. Cook, "Low-cost wireless force sensor design with applications in friction stir welding," 06 2012, pp. 70–75.
- [7] K. Takahashi, N. Suzuki, and E. Shamoto, "Identification of the model parameter for milling process simulation with sensor-integrated disturbance observer," *Precision Engineering*, vol. 78, pp. 146–162, 2022.
- [8] S.-I. Ao and H. Fayek, "Continual deep learning for time series modeling," *Sensors*, vol. 23, no. 16, 2023.
- [9] E. Salvato, G. Fenu, E. Medvet, and F. A. Pellegrino, "Crossing the reality gap: A survey on sim-to-real transferability of robot controllers in reinforcement learning," *IEEE Access*, vol. 9, pp. 153 171–153 187, 2021.
- [10] P. M. Scheikl, E. Tagliabue, B. Gyenes, M. Wagner, D. Dall'Alba, P. Fiorini, and F. Mathis-Ullrich, "Sim-to-real transfer for visual reinforcement learning of deformable object manipulation for robot-assisted surgery," *IEEE Robotics and Automation Letters*, vol. 8, no. 2, pp. 560–567, 2023.
- [11] D. Zhang, W. Fan, J. Lloyd, C. Yang, and N. F. Lepora, "One-shot domain-adaptive imitation learning via progressive learning applied to robotic pouring," *IEEE Transactions on Automation Science and Engineering*, pp. 1–14, 2022.
- [12] Y. Zhang and B. D. Davison, "Deep spherical manifold gaussian kernel for unsupervised domain adaptation," in *2021 IEEE/CVF Conference on Computer Vision and Pattern Recognition Workshops (CVPRW)*. Los Alamitos, CA, USA: IEEE Computer Society, Jun 2021, pp. 4438–4447.
- [13] Y. Zhao, C. Liu, Z. Zhiwei, K. Tang, and D. He, "Reinforcement learning method for machining deformation control based on meta-invariant feature space," *Visual computing for industry, biomedicine, and art*, vol. 5, p. 27, 11 2022.
- [14] J. Xing, T. Nagata, K. Chen, X. Zou, E. Neftci, and J. L. Krichmar, "Domain adaptation in reinforcement learning via latent unified state representation," *CoRR*, vol. abs/2102.05714, 2021.
- [15] M. Ragab, E. Eldele, W. L. Tan, C.-S. Foo, Z. Chen, M. Wu, C.-K. Kwok, and X. Li, "Adatime: A benchmarking suite for domain adaptation on time series data," *ACM Trans. Knowl. Discov. Data*, vol. 17, no. 8, May 2023.
- [16] K. Li, M. Chen, Y. Lin, Z. Li, X. Jia, and B. Li, "A novel adversarial domain adaptation transfer learning method for tool wear state prediction," *Knowledge-Based Systems*, vol. 254, p. 109537, 2022.
- [17] C.-B. Chou and C.-H. Lee, "Generative neural network-based online domain adaptation (GNN-ODA) approach for incomplete target domain data," *IEEE Transactions on Instrumentation and Measurement*, vol. 72, pp. 1–10, 2023.
- [18] K. Zhang, B. Scholkopf, K. Muandet, and Z. Wang, "Domain adaptation under target and conditional shift," in *International Conference on Machine Learning*, 2013.
- [19] H. Jung and S. Oh, "Gaussian process and disturbance observer based control for disturbance rejection," in *2022 IEEE 17th International Conference on Advanced Motion Control (AMC)*, 2022, pp. 94–99.
- [20] F. Golemo, A. A. Taiga, A. Courville, and P.-Y. Oudeyer, "Sim-to-real transfer with neural-augmented robot simulation," in *Proceedings of The 2nd Conference on Robot Learning*, ser. Proceedings of Machine Learning Research, A. Billard, A. Dragan, J. Peters, and J. Morimoto, Eds., vol. 87. PMLR, 29–31 Oct 2018, pp. 817–828.
- [21] P. F. Christiano, Z. Shah, I. Mordatch, J. Schneider, T. Blackwell, J. Tobin, P. Abbeel, and W. Zaremba, "Transfer from simulation to real world through learning deep inverse dynamics model," *CoRR*, vol. abs/1610.03518, 2016.
- [22] K. Wang, J. Ma, K. L. Man, K. Huang, and X. Huang, "Sim-to-real transfer with domain randomization for maximum power point estimation of photovoltaic systems," in *2021 IEEE International Conference on Environment and Electrical Engineering and 2021 IEEE Industrial and Commercial Power Systems Europe (EEEIC / I&CPS Europe)*, 2021, pp. 1–4.
- [23] S. Eleftheriadis, O. Rudovic, M. P. Deisenroth, and M. Pantic, "Gaussian process domain experts for model adaptation in facial behavior analysis," in *2016 IEEE Conference on Computer Vision and Pattern Recognition Workshops (CVPRW)*. Los Alamitos, CA, USA: IEEE Computer Society, Jul 2016, pp. 1469–1477.
- [24] M. Kaspar, J. D. Muñoz Osorio, and J. Bock, "Sim2real transfer for reinforcement learning without dynamics randomization," in *2020 IEEE/RSJ International Conference on Intelligent Robots and Systems (IROS)*, 2020, pp. 4383–4388.
- [25] S. Jiang, J.-C. Pang, and Y. Yu, "Offline imitation learning with a misspecified simulator," in *Proceedings of the 34th International Conference on Neural Information Processing Systems*, ser. NIPS'20, H. Larochelle, M. Ranzato, R. Hadsell, M. Balcan, and H. Lin, Eds., vol. 33, Red Hook, NY, USA, 2020, pp. 8510–8520.
- [26] T. Giorgino, "Computing and visualizing dynamic time warping alignments in R: the dtw package," *Journal of statistical Software*, vol. 31, pp. 1–24, 2009.
- [27] E. Armarego and R. Brown, *The Machining of Metals*. Prentice-Hall, 1969.